Diffusion-reaction model for *Drosophila* embryo development

R. Allena[1], J. J. Muñoz[2] and D. Aubry[1]

(1)Laboratoire MSSMat UMR CNRS 8579, Ecole Centrale Paris

Grande Voie des Vignes

92295 Châtenay-Malabry (France)

+33 (0)1 41 13 17 05

+33 (0)1 41 13 14 42

rachele.allena@ecp.fr

denis.aubry@ecp.fr

(2) Laboratori de Càlcul Numèric, Universitat Politècnica de Catalunya

Jordi Girona 1-3

E-08034 Barcelona (Spain)

+34 93 401 7760

j.munoz@upc.edu

Abstract During the early stages of gastrulation in *Drosophila* embryo, the epithelial cells composing the single tissue layer of the egg undergo large strains and displacements. These movements have been usually modeled by decomposing the total deformation gradient in an (imposed or strain/stress dependent) active part and a passive response. Although the influence of the chemical and genetic activity in the mechanical response of the cell has been experimentally observed, the effects of the mechanical deformation on the latter has been far less studied, and much less modeled. Here, we propose a model which couples morphogen transport and the cell mechanics during embryogenesis. A diffusion-reaction equation is introduced as an additional mechanical regulator of morphogenesis. Consequently, the active deformations are not directly

imposed in the analytical formulation, but they rather depend on the morphogen concentration, which is introduced as a new variable. In this work, we show that similar strain patterns to those observed during biological experiments can be reproduced by properly combining the two phenomena. Additionally, we use a novel technique to parameterize the embryo geometry by solving two Laplace problems with specific boundary conditions. We apply the method to two morphogenetic movements: ventral furrow invagination and germ band extension. The matching between our results and the observed experimental deformations confirms that diffusion-reaction of morphogens can actually be controlling large morphogenetic movements.

1 Introduction

During the development of multi-cellular organisms there is a combination of a biochemical pattern [17] and mechanical movements that shape the embryo [24]. The interdependence of these two contributions adds an enormous difficulty to the complete understanding of the essential developmental phases. The *Drosophila* embryo is an interesting biological model, which has been amply studied in the last decades from both the experimental and the numerical points of view. Furthermore, biologists have been able to observe the genetic control of the successive steps of embryogenesis [16], which has been often related to the expression of specific genes for each morphogenetic movement [29].

In the embryo, cells do not act alone but rather collaborate with neighboring cells and rearrange their configuration in order to maintain the highly organized structure of the system. This is a fascinating scientific aspect because it requires having a multiscale approach: at the cellular scale (microscopic) and at the tissue scale (macroscopic).

While active cells deform locally under genetic signalling, their interaction and activity are mediated and globally transferred to their neighboring cells. The stress state of the cell has been hypothesized as a potential source of communication

[35, 42, 52]. However, diffusion patterns have been observed in developing systems such as the zebra fish [26], the fly wing [23] or in *Drosophila* syncytial embryo [19]. It has been noticed that the morphogen diffusion has an effect in gene expression, with subsequent implication in embryogenesis at the tissue level. In the *Drosophila* embryo, the Dorsal morphogen has been reported to have an immediate effect on the expression of the important genes twist and snail [47, 29]. These are responsible of the main large deformations that take place during embryo gastrulation such as ventral furrow invagination (VFI) and germ band extension (GBE) [29]. The aim of the present work is to verify whether the coupling of the cell mechanics and the diffusion process may yield the observed deformations during the development of the *Drosophila* embryo.

Recently, numerical modeling in embryo biomechanics has played an important role. A major step has been the use of a deformation gradient decomposition [44, 46]. This method couples the large active and the passive deformations occurring to the cells. The former is usually considered a purely local kinematical process proper to each cell and therefore directly introduced into the formulation according to the experimental observations. The latter is instead a (visco)elastic response of the surrounding tissue, which requires then a mechanical analysis. Nevertheless, recent biological experiments have shown that the active deformations may depend on the passive deformations or on the stresses as a feedback mechanism [7, 16], and some numerical models have introduced phenomenological laws in order to take into account this potential aspect [35, 42, 52].

1.1 Morphogens activity

Despite the important progresses and the results obtained in the context of the embryogenesis, there is still a relevant aspect that has not been so much explored from a numerical point of view: the process by which the active individual deformations of the cells take place. This is actually a complex process, which has been experimentally studied by analyzing the presence inside the cells of specific morphogens.

Morphogens are proteins that may regulate the expression of target genes. They are believed to also provide positional information to specialized cell types within a tissue [2]. From experimental observations, it has been found that they spread from a localized source and form a concentration gradient across a developing tissue [19, 23, 26]. Morphogens are able to induce or maintain the expression of different target genes at distinct concentration thresholds. Consequently, cells close to the source of morphogens will show high gene expression depending on the concentration threshold of the target gene. Moreover, after the gene expression has taken place, the cell activity may induce active deformations that in turn may modify the concentration levels. As we show in the results section, this feedback mechanism is relevant for the control of the observed cell deformations.

The presence of diffusion phenomena in pattern formation of biological systems has already been investigated [53, 55] and it has led to a fruitful research line on the formation of diffusion-reaction geometrical pattern (see for instance a review in [31] and [36]. In these studies though, the concentration affects indeed the deformation pattern, but the influence of the latter on the concentration profile is rather low. Hence, the biological systems consisted of tissues which were mechanically sensible to the chemical concentration, but where the diffusion-reaction equations were unaffected by the resulting deformations.

In the last decades a series of numerical models that combine growth and pattern formation have been proposed in the literature by different authors. Among them we mention the general approaches of Crampin [14] and Neville [37], and the more applied works of Oster [39], who uses mesenchymal cells and a substrate to model their motility through strain dependent diffusion, and Umilis [54], in which a large number of genes and product proteins is employed to simulate pattern formation during *Drosophila* segmentation process. Most of these studies deal with two-dimensional or one-dimensional pattern formation on a growing tissue. However, our main concern is to explore the influence of relatively simple chemical reactions equations on cells shape changes that occur in the three-dimensional space as for the real embryo.

The modeling of diffusion-mechanical coupled problems with large deformations and displacements during embryo development has been so far very little studied. We can point out some related and interesting works in the context of plant growth [5], where diffusion equations are also coupled with a growth process, wound healing [22], cardiac tissue with concentrations that depend on the electric intensity or the stresses ([10] and [41] respectively), or teeth growth [45]. In all these models, diffusion-reaction equations have an effect on the rest length, active stresses, or tissue growth. Our model is in fact related to the latter case, since the morphogen concentration mediates the cellular shape changes, but without actually considering any growth process. In addition, we emphasize that although we also resort to an underlying diffusion-reaction equation, the morphogen concentrations are in turn also highly affected by the model kinematics due to the presence of large deformations and displacements in the biological structure.

1.2 Interactions between morphogens activity and mechanics

To accomplish our main objective mentioned above, an extension of our previous model [4] is introduced in order to include a diffusion-reaction as an additional mechanical regulator of morphogenesis, and to consider an evolution law that relates the active deformations and the morphogen concentration. We show that similar strain patterns to those observed during biological experiments can then be reproduced by properly combining the two phenomena.

Additionally, we use a technique that we have recently proposed [3] to parameterize the embryo geometry. This method uses the solution of two Laplace boundary problems to define the parameters that will be employed in the definition of our active deformations. Such boundary value problem can be identified with an electrostatic problem, and although we do not directly couple such potential with our mechanical and diffusion-reaction variables, we note that the presence of the electric field may be additionally taken into account in future studies. Indeed, it has been shown that the electric field may strongly influence cell signaling [48]. We therefore believe that the coupling between our electrostatic problem and the chemical and mechanical fields has a large potential in embryo modeling.

2. Harmonic parameterization of the embryo geometry

The three-dimensional geometry of the Drosophila embryo has been constructed from an interior and exterior ellipsoid in order to obtain a realistic shape. (Fig. 1). The major axis is 500μm long, while the cross axes CE and DF are respectively

175μm and 165μm long. The thickness is not constant, but it varies between 15μm<h<40μm. Such variations have been also observed in real embryos.

It will become useful in subsequent sections to accurately parameterize this geometry. We have therefore defined a local curvilinear coordinates system described by the three parameters V_θ, V_z and V_ζ, as represented in Fig. 2a. Each one of them is computed by solving Laplace's equation on the epithelium with appropriate boundary conditions [25]. Similar developments have been proposed in literature by Marchandise *et al* [32] who use the term harmonic which we find now more appropriate than electric as in our previous work [3]. In the next sections, we briefly describe how we numerically build the normal and the tangential coordinates.

2.1 Normal and tangential variables

Let $\partial\Omega_e$, $\partial\Omega_i$ and Σ_0 be respectively the outer, the inner and the middle surface of the *irregular* ellipsoid Ω. An harmonic variable $V_\zeta(x,y,z)$ within the thickness of the membrane is defined as follows

$$\begin{cases} \Delta V_\zeta = 0 \text{ inside } \Omega \\ V_\zeta = +\dfrac{h}{2} \text{ on the external boundary } \partial\Omega_e \\ V_\zeta = -\dfrac{h}{2} \text{ on the internal boundary } \partial\Omega_i \end{cases} \qquad (1)$$

where *h* is the thickness of the ellipsoid. As shown in Fig. 2b, the surface $V_\zeta = 0$ provides in a good approximation of the middle surface Σ_0.

From the calculated variable V_ζ, the normal vector $\boldsymbol{n}_0$ to the shell middle surface $V_\zeta = 0$ can be estimated as follows

$$\boldsymbol{n}_0 \cong \frac{\nabla V_\zeta}{\left\|\nabla V_\zeta\right\|} \qquad (2)$$

To have a complete system of curvilinear coordinates, we need now to find the two tangential parameters, V_θ and V_z. The latter one corresponds to the global cylindrical variable *z*, while we will compute V_θ by using similar boundary value problems to the one defined in Eq. (1). However, since the hollow geometry of the embryo may have only two boundaries (the internal and external surfaces), special care must be taken when defining the boundary conditions for V_θ [8][18]. We will introduce a fictive slit surface $\partial\Omega_{s_\theta}$, defined by {*z*=0, *y*<0}, so that the coordinate which runs circumferentially around the membrane making a closed loop is assumed to be discontinuous at $\partial\Omega_{s_\theta}$.

More precisely, V_θ is chosen to be the solution of the following Laplace's equation and boundary conditions with $[\bullet]$ standing for the jump of the quantities across the slit:

$$\begin{cases} \Delta V_\theta = 0 \text{ inside } \Omega_0 \\ [V_\theta] = 2\pi \text{ across the cut } \partial\Omega_{s_\theta} \\ \dfrac{\partial V_\theta}{\partial \boldsymbol{n}} = 0 \text{ on } \partial\Omega_e \text{ and } \partial\Omega_i \end{cases} \qquad (3)$$

where $\boldsymbol{n}$ is the normal vector to the inner and outer boundaries of the embryonic tissue. The boundary problems in (1) and (3) are solved using finite elements. The associated vectors $\boldsymbol{V}_\theta$ and $\boldsymbol{V}_z$ that complete the curvilinear basis are obtained, as similarly as for the normal vector $\boldsymbol{n}_0$ (Eq. (2)), as follows

$$\begin{cases} \boldsymbol{V}_\theta = \dfrac{\nabla V_\theta}{\left\|\nabla V_\theta\right\|} \\ \boldsymbol{V}_z = \dfrac{\nabla V_z}{\left\|\nabla V_z\right\|} \end{cases} \qquad (4)$$

2.2 Parameterization of the intermediate configuration

Now that the system of curvilinear coordinates has been completed, any point $\boldsymbol{p}\left(V_\theta, V_z, V_\xi\right)$ through the thickness of the embryo can be analytically located (Fig. 2a). Actually, let $\boldsymbol{p}_0\left(V_\theta, V_z\right)$ be a point on the middle surface of the ellipsoid such that $V_\zeta(x, y, z) = 0$, then we can write

$$\boldsymbol{p}\left(V_\theta, V_z, V_\zeta\right) = \boldsymbol{p}_0\left(V_\theta, V_z\right) + V_\zeta \boldsymbol{n}_0\left(V_\theta, V_z\right) \qquad (5)$$

As it will explained in the next section, and as a consequence of a morphogen concentration, each point where such concentration is different from zero moves from its initial position $\boldsymbol{p}$ to an *intermediate position* $\bar{\boldsymbol{x}}$, with a similar expression to (5) but using a modified parameterization $\left(\bar{V}_\theta, \bar{V}_z, V_\zeta\right)$:

$$\boldsymbol{p}\left(\bar{V}_\theta, \bar{V}_z, V_\xi\right) = \boldsymbol{p}_0\left(\bar{V}_\theta, \bar{V}_z\right) + V_\xi \boldsymbol{n}_0\left(\bar{V}_\theta, \bar{V}_z\right) \qquad (6)$$

The relations between parameters $\left(\bar{V}_\theta, \bar{V}_z, V_\zeta\right)$ and $\left(V_\theta, V_z, V_\zeta\right)$ determine the shape of the active displacements from $\boldsymbol{p}$ to $\bar{\boldsymbol{x}}$, and will be specified in Section 4 for each morphogenetic movement. For later use in the analysis of the elastic equilibrium, it will become useful to derive the expression of the active deformation gradient $\boldsymbol{F}_a$, which is given by [46]

$$\boldsymbol{F}_a = \frac{\partial \bar{\boldsymbol{x}}}{\partial \boldsymbol{p}} = \frac{\partial \bar{\boldsymbol{x}}}{\partial V_\theta} \otimes \boldsymbol{\nabla}_p V_\theta + \frac{\partial \bar{\boldsymbol{x}}}{\partial V_z} \otimes \boldsymbol{\nabla}_p V_z + \frac{\partial \bar{\boldsymbol{x}}}{\partial V_\zeta} \otimes \boldsymbol{\nabla}_p V_\zeta \qquad (7)$$

The vectors $\frac{\partial \bar{\boldsymbol{x}}}{\partial V_\theta}$, $\frac{\partial \bar{\boldsymbol{x}}}{\partial V_z}$ and $\frac{\partial \bar{\boldsymbol{x}}}{\partial V_\zeta}$ form the *covariant basis* at $\bar{\boldsymbol{x}}$, and are explicitly function of the *covariant basis* at $\boldsymbol{p}$ formed by the vectors $\frac{\partial \boldsymbol{p}}{\partial V_\theta}$, $\frac{\partial \boldsymbol{p}}{\partial V_z}$ and $\frac{\partial \boldsymbol{p}}{\partial V_\zeta}$. The

latter are in turn computed from the *contravariant basis* at $\boldsymbol{p}$ according to the following relationship

$$\frac{\partial \boldsymbol{p}}{\partial V_\theta} = \frac{\nabla_{\boldsymbol{p}} V_z \times \nabla_{\boldsymbol{p}} V_\zeta}{g^{\boldsymbol{p}}} \qquad (8)$$

with $g^{\boldsymbol{p}} = \left(\nabla_p V_\theta, \nabla_p V_z, \nabla_p V_\zeta\right)$ the determinant of these three vectors.

3. Coupled diffusive-kinematic model

In this section we introduce the governing equations and the evolution law of our chemo-mechanical system. We consider the embryonic tissue as a continuum domain under large deformations. The decomposition of the deformation gradient is used in order to take into account both the active and the passive components. The latter is assumed elastic, whereas the former, contrarily to previous models [4, 34], depends here on the morphogen concentration. More specifically, the total observed deformation of the tissue is the result of the following steps:

- An active deformation that depends on the morphogen concentration in a simple manner. The pattern of the active deformation is kept constant, whereas the rate of it its intensity depends linearly on the concentration level. Section 3.1 formalises this dependence.
- A superimposed elastic deformation that resolves the kinematic incompatibilities of the active deformation. As described in Section 3.2, the amount of the latter is found using standard equilibrium of elastic continua.

3.1 Chemo-mechanical framework

3.1.1. Definition of intermediate configuration

During morphogenesis, some cells at specific regions of the embryo undergo transformations in shape, which are apparently not triggered by the stress state of the tissue. These individual strains, represented by the active deformation gradient $\boldsymbol{F}_a$, change according to each morphogenetic movement, and may be kinematically incompatible (i.e., they lead to superposition of the cellular domains or discontinuities). If material compatibility is enforced at the final observed configuration, the active deformation $\boldsymbol{F}_a$ must be complemented with the so-called passive deformation $\boldsymbol{F}_m$. As a result, the total deformation gradient of the tissue $\boldsymbol{F}$ is decomposed according to the following multiplicative form:

$$\boldsymbol{F} = \boldsymbol{F}_m \boldsymbol{F}_a \qquad (9)$$

The passive deformation gradient $\boldsymbol{F}_m$ is determined by the elastic stress response of the cells and the mechanical equilibrium, while $\boldsymbol{F}_a$ is computed at each point $\boldsymbol{p}$ according to (6). In the present work, $\boldsymbol{F}_a$ will be restricted to have the following form

$$F_a = \hat{F}_a(\alpha) \qquad (10)$$

where $\hat{F}_a$ and α are the *deformation mode* and the *intensity active factor*, respectively. They control the *shape* and the *magnitude* of the active deformation, respectively.

The specific form of $\hat{F}_a$ determines the actual imposed deformation. In general, this form will be defined through a set of relations between $\left(\bar{V}_\theta, \bar{V}_z, V_\zeta\right)$ and $\left(V_\theta, V_z, V_\zeta\right)$, which are now also dependent on the variable α:

$$\bar{V}_\theta = \bar{V}_\theta\left(V_\theta, V_z, V_\zeta, \alpha\right) \quad (11a)$$

$$\bar{V}_z = \bar{V}_z\left(V_\theta, V_z, V_\zeta, \alpha\right) \quad (11b)$$

The actual expressions of these functions will be explicitly given for each morphogenetic movement in Section 4. In all cases, the evolution of factor α is driven by chemical diffusion, as will be described in the next paragraphs.

We note that this formulation is in contrast with other growth process suggested in the literature, where the active deformations depend on the Piola-Kirchhoff [30] or the Kirchhoff stresses [20]. In our case instead, the pattern of the active deformations remains prescribed, while its intensity is modulated with the morphogen concentration. By resorting to such prescribed patterns we are reducing the flexibility to model other potential cell shape changes. Nevertheless, we show in our results that by using suitable choices of these patterns we can reproduce the local cellular movements such as the apical constriction during the VFI or the intercalation process during the GBE, without having to explicitly model the cytoskeleton or the cell-cell contact at the membrane.

3.1.2. Evolution law and diffusion-reaction equations

The chemical and the mechanical fields are coupled with a simple linear relationship between the rate of the intensity active factor α and the actual concentration per unit of deformed volume *c* as follows

$$\frac{d\alpha}{dt} = \beta \cdot c \qquad (12)$$

where β is a positive constant. This equation is motivated by the following three facts: i) at points with larger morphogen concentration the genes will be more likely to trigger the driving active forces, ii) we aim to achieve a homeostatic state, with $c\approx 0$, where no further active deformations are introduced, and iii) at the end of the morphogenetic movement, when $c=0$, the value of α must remain unchanged, i.e., the process will not be reversed. This latter fact has prevented us from setting a linear relationship between α and c. The parameter β controls the influence of the concentration onto the active deformations, which is a consequence of multiple factors. In the two morphogenetic movements analyzed here we have assigned a single value to β such that the deformed configuration resembles the observed one. This is of course a preliminary simple choice which can be modified in the future.

We note that, since $c\geq 0$, α will always increase. However, its rate may increase or decrease according to the concentration rate itself. We recognize that as far as $c\neq 0$, α will keep increasing, which seems *a priori* unrealistic. In fact, equation (12) is a linear approximation of multiple concurrent complex phenomena that occur during a larger time-span than the duration of our analysis. Our model does not aim to fully reproduce all this myriad of processes with such a linear relationship, and consequently will become more approximated during the end-time instants. We will limit our attention and conclusions to a subinterval of this whole period, where equation (12) seems better justified and better reproduces the experimental observations.

We define an *active region* as the domain where $\alpha\neq 0$, and therefore a region where some active deformations are present. We will assume an initial condition where the morphogen concentration is uniform on a restricted region. Due to Eq.

(12), such region will be subjected to active deformations, but due to diffusion-reaction of this morphogen, the active region will vary its extension as a function of time.

Let us consider the motion $\Omega_p \to \Omega_x$ from the reference to the actual configuration and assume that the concentration *c* follows a diffusion-reaction equation at the instant *t*. Thus, if div_x and ∇_x are respectively the divergence and the gradient with respect to the actual position $\boldsymbol{x}$, the balance of morphogen onto a control volume yields the following equation

$$\frac{dc}{dt} + c\, div_x \boldsymbol{v} = div_x \left(k_D \nabla_x c \right) + k_R c \quad (13)$$

with $\boldsymbol{v}$ the velocity of the material, k_D the diffusivity scalar constant and k_R the chemical reaction coefficient.

For large deformations problems, and with the aim of spatially discretizing the model with finite elements, we will express the above differential equation with respect to the reference configuration. Recalling that $\frac{dJ}{dt} = J\, div_x \boldsymbol{v}$ (with $J = \det \boldsymbol{F}$), and $\nabla_{\boldsymbol{x}} c = \boldsymbol{F}^{-T} \nabla_{\boldsymbol{p}} c$, and according to Piola's identity $div_{\boldsymbol{x}} \boldsymbol{a} = \frac{1}{J} div_{\boldsymbol{p}} \left(J \boldsymbol{F}^{-1} (\boldsymbol{a}) \right)$ [33] where $\boldsymbol{a}$ is any vector, we have that Eq. (13) turns into

$$\frac{d(Jc)}{dt} = div_p \left(J\, k_D\, \boldsymbol{C}^{-1} \left(\nabla_p c \right) \right) + J k_R c \qquad (14)$$

where $\boldsymbol{C} = \boldsymbol{F}^T \boldsymbol{F}$ is the Cauchy-Green deformation tensor. We emphasize that we are solving the reaction-diffusion equation onto a deformable domain, and therefore some additional terms have arisen with respect to diffusion-reaction equations on a fixed domain. We note that the effects of the medium deformation onto the concentration evolution are twofold. On one hand, the initial scalar diffusion term k_D is now replaced by an anisotropic diffusion tensor $J\, k_D\, \boldsymbol{C}^{-1}$.

Thus, for highly deformed tissues, the diffusion term decreases along the principal direction of deformation. On the other hand, we can identify a reaction term equal to $c\left(Jk_R - \frac{dJ}{dt}\right)$. Consequently, if the material is compressed ($\frac{dJ}{dt} < 0$), we will observe that the morphogen concentration augments due to the increase of $\left(Jk_R - \frac{dJ}{dt}\right)$.

Due to the diffusion-reaction process in Eq. (14) and to the evolution law in Eq. (12), we will observe a gradient of the active deformation. This is in contrast to our previous works [4, 34] where the intensity factor α was assumed uniform throughout the active region.

The corresponding weak form of Eq. (14) is obtained in the usual manner: by multiplying this equation by the test concentration $\bar{c}$, so that, assuming vanishing concentration flux outside the embryo, we have

$$\int_{\Omega_p} \bar{c}\frac{d(Jc)}{dt}dV = -\int_{\Omega_p} Jk_D\left(\boldsymbol{C}^{-1}\left(\nabla_p \bar{c}\right), \nabla_p c\right)dV + \int_{\Omega_p} Jk_R \bar{c}c dV \qquad (15)$$

where $(\boldsymbol{a}, \boldsymbol{b})$ is the dot product of two vectors $\boldsymbol{a}$ and $\boldsymbol{b}$. Equation (15) will be discretized by a standard finite element method on the initial configuration.

3.1.3 Qualitative analysis of the model

Before detailing the numerical simulation on the full embryo, let us consider from a qualitative point of view the influence of the diffusion coefficient k_D and the reaction coefficient k_R. In order to illustrate and evaluate this specific aspect, we consider a one-dimensional domain $\infty < x < \infty$ with an initial active region at the center $(-1 \le x \le 1)$ that has a morphogen concentration $c = 1$ at $t=0s$. The differential equation (15) and the evolution law in (12) with β=0.1 have been symbolically solved with Mathematica®. Figs. 3a-b show the evolution of c and α,

respectively, as a function of time t and space x, in the case without reaction ($k_R=0$). As expected, it can be observed that morphogen concentration grows faster at the initial times, when c is higher. The region where the intensity active factor $\alpha \neq 0$ spreads outside the initial active region and increases monotonously as mentioned above.

It has been verified that when the chemical reaction is taken into account, $k_R \neq 0$, there is a morphogen production (consumption) when k_R is positive (negative), and consequently we have that α grows at faster (slower) rate. Fig. 3c-d show the evolution of c and α when $k_R<0$. In this case, c decreases much faster and the evolution of α is much slower.

These preliminary results confirm that when the activation factor α is driven by a diffusion-reaction equation, the activity that initially was concentrated in specific areas is transferred to neighboring zones. This concentration will affect the mechanical response of the system, and as it will be shown in the next section, the converse will also be true: the mechanical deformation will affect the morphogen concentration, similar to the mechanotransduction phenomenon observed within the tissue.

3.2 Mechanical equilibrium and behavior

Let $\boldsymbol{x}$ stands for the actual position of a material particle and $\boldsymbol{i}_m$ stands for a cartesian frame. Then the total deformation may be described by the deformation gradient

$$\boldsymbol{F} = \sum_{m=1,3} \frac{\partial \boldsymbol{x}}{\partial p_m} \otimes \boldsymbol{i}_m \qquad (16)$$

We remind that this total deformation gradient may be decomposed in its active and passive part according to Eq. (9). It is illustrative to contemplate two extreme situations: a) when the cell is completely free, without any boundary condition imposed, $\boldsymbol{F}_m = \boldsymbol{I}$ and $\boldsymbol{F} = \boldsymbol{F}_a$, i.e., the final deformation coincides with the active deformation itself, b) when the cell is fully constrained by other cells and by the boundary conditions, as in the case of the embryo, $\boldsymbol{F}_m$ is the actual response to the active deformation $\boldsymbol{F}_a$. In general, the two situations are mixed to provide the suitable final consistent deformation imposed by the continuity of the material.

The weak form of the mechanical equilibrium condition in the initial configuration Ω_p is expressed through the first Piola Kirchhoff stress $\boldsymbol{\pi}$ as follows

$$\int_{\Omega_p} Tr\left(\boldsymbol{\pi}\boldsymbol{D}_p\boldsymbol{w}^T\right)dV = \int_{\partial\Omega_p}\left(\boldsymbol{w}, f_s J\boldsymbol{F}^{-T}(\boldsymbol{n})\right)dS \quad (17)$$

where f_s indicates the pressures exerted on the inner and the outer surfaces of the embryo and $\boldsymbol{w}$ is a kinematically admissible displacement test function.

The first Piola-Kirchhoff tensors is computed as $\boldsymbol{\pi} = J_a\boldsymbol{F}_a^{-T}\boldsymbol{S}_m$ with $J_a = Det[\boldsymbol{F}_a]$. $\boldsymbol{S}_m$ is the Second Piola-Kirchhoff tensor with respect to the intermediate configuration and it is defined as

$$\boldsymbol{S}_m = \lambda Tr[\boldsymbol{E}_m]\boldsymbol{I} + 2\mu\boldsymbol{E}_m \quad (18)$$

where $\lambda = \dfrac{E}{(1+\nu)(1-2\nu)}$ and $\mu = \dfrac{E}{2(1+\nu)}$ are the Lamé material parameters, with E and ν the Young's modulus and Poisson's ratio, respectively. The Green-

Lagrange strain tensor $E_m = \frac{1}{2}(C_m - I)$, with $C_m = F_m^T F_m = F_a^{-T} F^T F F_a$, measures the elastic passive deformation.

By using a purely elastic model we are disregarding any viscous dissipative phenomenon and the viscous forces. It must be noted though that some elastic contribution does exist, as the experiments in [49] and in [16] show, where the original shape of the embryo is recovered when an imposed deformation is removed. Indeed, the viscoelastic nature of embryo epithelia is still a controversial debated issue, and in fact, while some researchers have modeled the Drosophila embryo resorting to solely fluid equations [40], others use a purely elastic tissue [53].

In our case, by considering a purely elastic material, the passive deformations that accommodate the kinematic incompatibilities of the active ones will induce some elastic stresses. We are aware that these may be actually different from a representative stress state of the cell. We show in our numerical results that the actual value of the stresses is proportional to the material stiffness, which can be just estimated for embryo tissue [57]. None the less, we have also compared in Section 4.1 our stress values from those reported in other models.

More importantly, the active deformations of our model are independent of the material properties, and are those that largely contribute to the total deformation. The aim of the present work is reproduce the active deformations and to analyze the plausibility of a diffusion driven mechanism. We do not intend to match the *in vivo* stresses, which to the authors' knowledge, have not been reported so far.

The equilibrium equation in (17) must be complemented with the particular boundary conditions. In the *Drosophila* embryo, they correspond to the vitelline

membrane contact conditions and the internal yolk volume preservation. Due to the irregular shape of the ellipsoid, these conditions prevent any rigid body motion. They are modeled by including additional terms in Eq. (17) (see [4] for further details).

In summary, mechanical and chemical phenomena are coupled according to the following dependences:

- The elastic deformation on the morphogen concentration *c*: $\boldsymbol{\pi}$ depends on $\boldsymbol{F}_a$, which is mediated by the active intensity factor α that depends on the morphogen concentration *c*;
- The morphogen concentration *c* on the total deformation: the diffusion equation depends on **C** and J, reflecting the fact that compressed areas will increase their concentration *c*.

The two equations in (15) and (17) are simultaneously solved through a multistep time integration and a Newton scheme for the displacement $\boldsymbol{u}$ and the morphogen concentration *c* at each time step.

4. Morphogenetic movements

The coupled mechanical-diffusion model and the parameterization of the active deformations developed in the previous sections will be here applied to two morphogenetic movements: the ventral furrow invagination (VFI) and the germ band extension (GBE).

In the last decades, these two movements have been amply studied from both the experimental and the numerical points of view. In fact, some interesting computer models have been proposed in literature [1, 11, 12, 15, 21, 34, 40, 42, 51, 52, 56]. However, in all these references, the cell activity is either imposed or a function of the stress state of the cell. In the present work instead, motivated by the presence

of diffusion profiles of Dorsal morphogen that control the expression of the genes twist and snail during the VFI and the GBE [29, 47] or the concentration profiles of Fgf8 and Dpp in other developmental processes [23, 26], we will reproduce the VFI and the GBE according to the evolution law in (12), the diffusion-reaction equation in (15) and the mechanical equilibrium in (17).

In all the following analyses we have assumed the constant representative values: *E=100Pa* [57], *ν=0.45*, $k_D = 10^{-9}\, m^2 s^{-1}$ and $\beta = 10^{-1}\, m^3 s^{-1} mol^{-1}$. However, due to a lack of experimental information, we have set $k_R=0$, except for the simulation of the VFI where a parametric analysis has been done.

4.1 Ventral furrow invagination (VFI)

The VFI is an orthogonal invagination that takes place along the ventral embryonic midline. It extends between 6% and 85% egg length and it involves about 800 cells that will become internalized. The movement is highly controlled by two developmental genes: twist and snail. Additionally, the former induces the ventral expression of Fog and T48 [27], two proteins that recruit RhoGEF2 to constrict a contractile actin-Myosin II network that leads to the deformation of the active cells [38]. The VFI is triggered by a series of synchronized cell changes in shape that provide the final form of this furrow [1, 13, 28, 29, 50]. Similarly to our previous works [4], the apical constriction along the transversal section of the embryo is the only responsible of VFI. Apical constriction occurs primarily through the contraction of cytoskeletal elements and, specifically for the *Drosophila* embryo, the actin-myosin filaments. It consists in the contraction of the apical basis of the cells, which is in contact with the vitelline membrane, and it causes the cells to take a wedged shape.

Such deformation can be reproduced by applying the intermediate position in Eq. (6) and particularizing Eq. (11) to the following expressions:

$$\bar{V}_\theta = V_\theta + \alpha \frac{2V_\varsigma}{h} m(V_\theta) \qquad (19a)$$

$$\bar{V}_z = V_z \qquad (19b)$$

where $m(V_\theta)$ is a periodic function that mimics the cell boundaries by appropriately modulating the intensity of the active deformation. Its explicit expression is:

$$m(V_\theta) = 2\left[\frac{V_\theta}{V_{\theta\_cell}} - \frac{1}{2} - round\left(\frac{V_\theta}{V_{\theta\_cell}} - \frac{1}{2}\right)\right] \qquad (20)$$

where V_{θ_cell} corresponds to the angular extension of a material cell and *round* is the classical step function which gives the integer number of $\left(\frac{V_\theta}{V_{\theta\_cell}} - \frac{1}{2}\right)$.

This function subdivides the embryonic tissue into several sub-domains corresponding to the real cells. By using this periodic function we can evaluate the individual cellular deformations. It depends on the hypothesized dimensions of a real cell of the embryo that have been set equal to $15\mu m$ along $\boldsymbol{V}_\varsigma$ and $10\mu m$ along $\boldsymbol{V}_\theta$ and $\boldsymbol{V}_z$. In Fig. 4a**,** it is possible to observe the physical distribution of the pseudo-cells along the transversal section of the embryo. Each white domain represents a cell, while the black domains are triggered by the smoothing effect of the Heaviside function by which the material cells are obtained [4].

The values of the intensity factor α are determined by the evolution law in Eq. (12). By inserting Eq. (19) into Eq. (6), the active deformation gradient $\boldsymbol{F}_a$ can be then computed according to Eq. (7).

At the initial time, a uniform non-zero concentration is introduced in a restrained region of the embryo, as it is observed in reality. Fig. 5 shows this region with the

initial conditions for the concentration *c*. Such area is obtained using a Heaviside function that is equal to one in the region with non-zero concentration values and equal to zero everywhere else. The discontinuities of this function have been smoothed to ease the computations [4].

The successive steps of the VFI are shown in Fig. 6a, b and c. The embryonic tissue is more constricted in the area corresponding to the active region, due to the higher initial morphogen concentration. As the diffusion phenomenon takes place, the initial concentration decreases. Thus, at $t = 0s$ we have a concentration $c = 1mol \cdot m^{-3}$ in the center of the active region (Fig. 6a), while at the end of the simulation ($t = 1s$) we find $c = 0.36mol \cdot m^{-3}$ (Fig. 6c). The experimental values of Dorsal morphogen concentration in the embryo during the VFI are not detailed, and just the general profiles can be found in the literature [47]. Furthermore, the value of parameter β, which controls the influence of the concentrations on the active deformations, is hard to measure and has just been estimated in our simulations.

The general trend of the strains due to the diffusion phenomenon agrees with the experimental observations. Indeed, while the morphogen concentration reduces during the simulation, the active intensity factor increases and consequently the final strain occurring to the cells (Fig. 7a). At the initial configuration (Fig. 4a), the cells show a columnar shape, while at $t = 1s$, once the furrow has formed (Fig. 4b**),** the apical constriction is clearly evident, especially for the cells in the active region. Fig. 8 shows the value of the total stretching along $\boldsymbol{V_\theta}$, which is computed as the projection of the Cauchy-Green deformation tensor $\boldsymbol{C}$ along $\boldsymbol{V_\theta}$ as follows

$$\left(C\left(V_\theta\right), V_\theta\right) \quad (21)$$

We find that the final maximal stretching for the mechano-diffusion model at the apex of the invagination is equal to 0.74 (Fig. 8b), which is almost double compared to the one found in our previous simulation of the VFI with the imposed active deformations (0.32) (Fig. 8a) [3]. According to the chosen dimensions of a real cell, we can estimate that the maximal apical constriction at the apex of the furrow is equal to $7.5\mu m$. In general, the final strain simultaneously depends on the initial position of the cell as well as on the diffusion phenomenon here implemented.

Although no *in vivo* stresses have been reported in the literature, we have computed the stresses along the direction $\boldsymbol{V}_\theta$, that is, the value of ($\mathbf{S}_m$ ($\boldsymbol{V}_\theta$), $\boldsymbol{V}_\theta$) at point E in Fig.1b, and compared the values with those reported in [6]. From the expression of $\mathbf{S}_m$ in Eq. (18), we deduce that ($\mathbf{S}_m(\boldsymbol{V}_\theta),\boldsymbol{V}_\theta$)= λTr[$\mathbf{E}_m$]+2μ(($\mathbf{E}_m$ ($\boldsymbol{V}_\theta$),$\boldsymbol{V}_\theta$)-, which is directly proportional to the Young modulus *E*. We have plotted in Fig. 7a the evolution of ($\mathbf{S}_m(\boldsymbol{V}_\theta),\boldsymbol{V}_\theta$). For the value employed in our model, E=100Pa, the stress value approaches 400Pa (Fig. 7c,d). In order to compare this value with the tractions reported in [6, Fig. 4a], we convert our stress value into a traction per unit of μm depth and applied onto a cell width (15 μm), which yields a force of 6 nN, This value is between one and two orders of magnitude higher than the one in [6], which as the authors in the reference recognise, is proportional to the viscosity, which in turn may vary in different orders of magnitude. It is also worth noting that our stresses and forces monotonically increase, while those in [6] have a parabolic trend. This is in agreement with the different material model considered, as discussed in Section 3.2: while the forces in [6] are proportional to the strain rate, ours are proportional to the accumulated elastic strain.

We also remark that, as pointed out by [9], the elongation of the invaginating tissue on both sides of the furrow towards the midline could be the direct cause of

the antero-posterior tensile force deforming the germ band in the early fast phase of its extension. Therefore, the VFI, as well as other three morphogenetic movements (cephalic furrow formation, posterior midgut invagination and amnioserosa cell elongation), could be a good candidate to contribute to the cells shape changes leading to the GBE, which are then considered as a passive response to the mechanical forces occurring during the VFI.

To conclude, we remark that the elastic deformations at any point in the initially non-active region of the tissue are originated by two contributions. For the regions where $\alpha=0$, the deformations in active areas with $\alpha\neq0$ will induce global elastic deformations. On the other hand, due to the diffusion phenomenon, α may eventually be positive and consequently superimpose an additional active deformation. Therefore, the total deformation at each point is due to the activity at neighboring cells, plus the active deformations that this point may have. This is in contrast to our previous simulation where the active deformations were exclusively localized in the initial active zone [4].

As a final and qualitative test, we have introduced the reaction term into Eq. (14) with $k_R=0.1s^{-1}$. The main objective of this specific simulation is to show that, as similarly as in Sec. 3.1.3, the reaction term may influence the global behavior of the biological system. Let us consider the point E of the ventral furrow as represented in Fig. 1. As expected, since $k_R>0$, we have a morphogen production which leads to an increase of the morphogen concentration c, as observed in Fig. 7b. This in contrast with the previous case (Fig. 7a) with $k_R=0$ and where c globally decreases due to the diffusion. For what concerns the evaluation of the active apical constriction, we remark that the final invagination is smaller than the model with $k_R=0$. Although further studies may be necessary, we believe that the proposed analysis can be considered as a first step to investigate the

mechanotransduction phenomenon. So far we have introduced a linear reaction term ($k_R\, c$), even though we are aware that for chemical analyses a non-linear term is usually involved ($k_R c^n$).

4.2 Germ band extension (GBE)

The germ band is located at the ventral region of the embryo and it starts to extend at the end of gastrulation [24]. This event leads to an elongation of the germ band of about 2.5 times its initial length. It is due to a convergent-extension movement of a population of cells at the central-lateral region of the embryo. This process is triggered by an intercalation of the cells that interpose themselves between their dorsal or ventral neighbors, resulting in a decrease of the number of cells along the dorsal-ventral axis and in an increase of the number of cells along the anterior-posterior axis [24]. Recently, it has also been shown that during the fast early phase, the GBE depends on cell shape change in addition to intercalation and that these changes in shape are a passive response to the mechanical forces caused by the invagination of the ventral tissue [43].

Here, since the cells are not individually modeled, we do not precisely simulate the intercalation process. Instead, we propose a continuous movement of compression-extension tangential to the middle surface of the blastoderm. Like in the VFI, the active deformations are introduced on a limited region of the embryo (Fig. 9a): the germ band at ventral region where the initial morphogen concentration is not zero. The intermediate position in Eq. (6) uses now the following particular expressions for $\bar{V}_\theta$ and $\bar{V}_z$:

$$\bar{V}_\theta = (1+\alpha) V_\theta \qquad (22a)$$

$$\bar{V}_z = (1+\alpha) V_z \qquad (22b)$$

The active deformation gradient $\boldsymbol{F}_a$ may be then computed by inserting these expressions into in Eq. (6) and evaluating Eq. (7).

The results for this simulation are plotted in Fig. 9b. As we can observe, the convergence-extension movement is evident even though the amplitude of the uniform compression from the dorsal to the ventral region is not so pronounced as in our previous work [4]. We can still notice the vortex movements forming towards the AP and the PP. Additionally, we have been able to evaluate the maximal value of the two active strains by projection of the Cauchy-Green deformation tensor along $\boldsymbol{V}_\theta$ (shortening, $\left(C\left(V_\theta\right), V_\theta\right)$) and along $\boldsymbol{V}_z$ (extension, $\left(C\left(V_z\right), V_z\right)$). We find respectively 0.06 for the convergence and 0.21 for the extension. Thus, if we consider the dimensions given in Section 4.1. for a single cell, we may observe an extension of each cell along $\boldsymbol{V}_z$ of about $2.1\mu m$ and a shortening along $\boldsymbol{V}_\theta$ equal to $0.6\mu m$.

Like in the VFI simulation, the morphogen concentration decreases during the diffusion phenomenon. Consequently, at $t=0s$ we find an initial maximal value of $c=1mol\cdot m^{-3}$ in the active region (Fig. 10a), while at the end of the simulation ($t=1s$), we have $c=0.08mol\cdot m^{-3}$ (Fig. 10c).

In Fig. 11, the trends of the intensity active factors, the two active strains, and the morphogen concentration at point E of Fig. 1 are reported as a function of *t*. As we can observe, the concentration *c* decreases while α progressively increases, which affects the tendency of the active deformations. The absolute value of the stretching in the directions of V_θ and V_z increases, but of course in the former case it is negative (shortening) while in the latter it is positive (lengthening).

5. Conclusions

We have coupled the diffusion-reaction equations on a deforming domain with the equilibrium equation of an elastic domain subjected to active deformations, which are in turn dependent on morphogen concentration. Additionally, a novel technique to parameterize the embryo geometry and obtain a set of covariant basis has been employed, which has allowed us to deduce the expressions of the concentration dependent active deformations. We have applied the model to simulate ventral furrow invagination and germ band extension in the *Drosophila* embryo.

Despite an increasing number of experiments analyzing the diffusion of morphogens, their effect onto the biological developing tissue has not been taken into account. Here, we couple these diffusion profiles with the mentioned two morphogenetic movements. The promising results show that the employed set of equations reproduces the trend of the active deformations observed during morphogenesis. Clearly, in order to obtain more realistic strains, the reaction term and the initial morphogen concentration should be regulated, especially for a consistent comparison with the experimental observations and values. Also, additional non-linear source terms are probably needed.

We recognise that by using a purely elastic material, some errors in the resulting stresses and the actual timing of the cellular response may have been introduced. We have though compared our stress values to those in [6], and remarked their good agreement. The lack of *in vivo* measurements, similar to those described for other morphogenetic movements in [19, 23, 26], does not allow us to give further rigorous quantitative analyses. Qualitatively, it is worth pointing out that the usual smooth profiles encountered in diffusion process may have sudden mechanical effects, as in the case of the FVI modeled here. These severe folds in the

epithelium may in turn drastically change the concentration profile, triggering non-smooth evolutions of the concentrations and strains, as shown in Fig. 6-7.

We note that due to the presence of the vitelline membrane in the *Drosophila* embryo it is not possible to measure stresses at the embryo epithelium. However, the development described here are easily extensible to other embryos such as the *Zebrafish*, where this data can be measured. We intend in future works to test our model in these embryos.

We note, that in contrast to the stress field, which is transferred nearly instantaneously, the diffusion process allows to match the timing of the morphogenetic movement, without artificially imposing a set of incremental active deformations. This is one of the features that has motivated the present work: the coupling of the active deformation with a physical quantity that enables to successfully control the rate and magnitude of the cell shape changes. In this paper, we have verified that the diffusion process is a plausible mechanism, able to govern the driving forces of the invagination process.

In our simulations, we have imposed a set of initial conditions for the concentrations, displacements, stresses and active deformations. We recognize that such conditions are certainly not always fully determined, and in fact correspond to the final conditions of other processes which we have not been modeled. For this reason, our comparisons have more a qualitative than a quantitative character. Nonetheless, the agreement between the observed deformations and our computations is certainly satisfactory. Furthermore, we point out that in our case, the active deformations are not directly imposed, but are a consequence of the morphogen diffusion and the evolution law proposed for the intensity factor α.

The simulations show that the dynamics of the diffusion process is compatible with an active genetic movement triggered by morphogens. The coupling between chemicals and mechanics through a diffusion-reaction in embryo development has not been attempted so far. The simulations presented here constitute then an original contribution for a better understanding of the whole three-dimensional problem. We are aware that the complex signalling process between mophogen concentrations and gene activity may further regulate the relation between embryo phenotype and its genotype. We have shown that without explicitly modeling the mechanotransduction path within the cells, morphogen activity may be included with simple rules that successfully match the complex synchronization between chemicals and mechanics during the embryo development.

Acknowledgments

This work has been financially supported by the Centre National de la Recherche Scientifique and by the Spanish ministry "Ministerio de Ciencia e Innovación" within the "José Castillejo" program, grant number 1078.

References

[1] Alberch O. et al., 1981. The mechanical basis of morphogenesis. Epithelial folding and invagination. Dev. Biology, 75, 446-462.

[2] Alberts B. et al, 2008. Molecular biology of the cell. Garland Science.

[3] Allena R. and Aubry D., 2011. A novel technique to parameterize shell-like deformations inside biological membranes. Computational mechanics, DOI: 10.1007/s00466-010-0551-8.

[4] Allena R., Mouronval A. –S., Aubry D., 2010. Simulation of multiple morphogenetic movements in the Drosophila embryo by a single 3D finite element model. JMBBM, 3: 313-323.

[5] Brière C. and Goodwin B.C., 1988. Geometry and dynamics of tip morphogenesis in Acetabularia, J. Theor. Biol, 131, 431-475

[6] Brodland GW, Conte V, Cranston PG, Veldhuis J, Narasimhan S, Hutson MS, Jacinto A, Ulrich F, Baum B, Miodownik M: Video force microscopy reveals the mechanics of ventral furrow invagination in Drosophila. PNAS 2010 Vol 107, 22111-22116

[7] Brouzés E., Farge E., 2004. Interplay of mechanical deformation and patterned gene expression in developing embryo. Curr. Opin. Genet. Dev., 14, 367-74.

[8] Brown M.L., 1983. Scalar potential in multiply connected beam. International Journal for Numerical Methods in Engineering, 20: 665-680.

[9] Butler L.C. *et al.,* 2009. Cell shape changes indicate a role for extrinsic tensile forces in Drosophila germ-band extension. Nature Cell Biology, DOI: 10.1038/ncb1894.

[10] Cherubini C., Filippi S., Nardinocchi P. and Teresi L., 2008. An electromechanical model of cardiac tissue: constitutive issues and electrophysiological effects. Progr. Byoph. Mol. Biol. 97:562-573.

[11] Clausi D.A., Brodland G.W., 1994. Embryonic tissue morphogenesis modeled by FEM. J. Biomech. Engin., 116 ,146-156.

[12] Conte V. et al., 2007. A 3D finite element model of ventral furrow invagination in the Drosophila Melanogaster embryo. J. of the mechanical behavior of biomedical materials. 1, 188-198.

[13] Costa M. et al., 1993. Gastrulation in Drosophila: cellular mechanisms of morphogenetic movements in: Bate M., Martinez-Arias A. (eds), The Development of Drosophila. Cold Spring Harbor Laboratory Press, New York, pp. 425–466.

[14] Crampin E.J., Gaffney E.A., Maini P.K., 1999. Reaction and diffusion on growing domains: scenarios for robust pattern formation. Bulletin of Mathematical Biology 61: 1093-1120.

[15] Davidson L. et al., 1995. How do *sea urchins* invaginate? Using biomechanics to distinguish between mechanisms of primary invagination. Development, 121, 2005-2018.

[16] Farge E., 2003. Mechanical induction of *twist* in the Drosophila foregut/stomodeal primordium. Current Biology, 13, 1365-1377.

[17] Gilbert S.F., 1994. Specification of cell fate by progressive cell-cell interactions. In: Gilbert S.F. (Ed.), Developmental Biology, Sinauer Associates, Inc. Publishersn Massachusetts, 575-622.

[18] Greenbaum A., Greengard L., McFadden G. B., 1993. Laplace's equation and Dirichlet-Neumann Map in Multiply Connected Domains. Journal of Computational Physics, 105: 267-278.

[19] Gregor T., Tank D.W., Wieschaus E.F., and Bialek W., 2007. Probing the limits to positional information. Cell, 130:153–164.

[20] Himpel G., Kuhl E., Menzel A., and Steinmann P., 2005. Computational modeling. of isotropic multiplicative growth. Comp. Mod. Eng. Sci., 8:119–134.

[21] Jacobson A.G. et al., 1986. Neurulation and cortical tractor model for epithelial folding. J. Embryol. Exp. Morph., 96,19-49.

[22] Javierre E., Moreo P., Doblaré M., Garcia-Aznar J.M., 2009. Numerical modeling of a mechano-chemical theory for wound contraction analysis. Int. J. Solids Struct., 46(20):3597-3606.

[23] Yu S.H., Burkhardt M., Nowak M., Ries J., Petrasek Z., Scholpp S., Schwille P., and Brand M., 2009. Fgf8 morphogen gradient forms by a source-sink mechanism with freely diffusing molecules. Nature 461: 533-536.

[24] Keller R. et al., 2000. Mechanisms of convergence and extension by cell intercalation. Philos. Trans. R. Soc. Lond. B. Biol. Sci., 355(1399), 897-922.

[25] Kellog O. D., 1953. Foundations of potential theory. Berlin Verlag Von Julius Springer,Dover.

[26] Kicheva A. et al, 2007. Kinetics of Morphogen Gradient Formation. Science 315: 521.

[27] Kolsh V., Seher T., Fernandez-Ballester G.J., Serrano L., Leptin M., 2007. Control of drosophila gastrulation by apical localization of adherense junctions and rhogef2. Science, 132:384-386.

[28] Leptin M., Grunewald B., 1990. Cell shape changes during gastrulation in Drosophila. Development, 110, 73-84.

[29] Leptin M., 1999. Gastrulation in Drosophila: the logic and the cellular mechanisms. EMBO J, 18, 3187-3192.

[30] Lubarda V.A. and Hoger A., 2002. On the mechanics of solids with a growing mass. Int. J. Solids Struct., 39:4627–4664.

[31] Maini P.K., Paintera K.J. and Phong-Chaub H.N., 1997. Spatial pattern formation in chemical and biological systems. J. Chem. Soc. Faraday Trans., 93(20): 3601-3610.

[32] Marchandise E., Carton de Wiart C., Vos W.G., Geuzaine C., Remacle J.-F., 2011. High-quality remeshing using harmonic maps Part II : Surfaces with high genus and of large aspect ratio. IJNME, DOI : 10.1002/nme.3099

[33] Marsden J.E. and Hughes T.J.R., 1983. Mathematical foundations of elasticity. Prentice Hall.

[34] Muñoz J.J. et al., 2007. A deformation gradient decomposition method for the analysis of the mechanics of morphogenesis. Journal of Biomechanics, 40: 1372-1380.

[35] Muñoz J. et al., 2010. Stress-dependent morphogenesis: continuum mechanics and truss systems. Biomechanics and modeling in mechanobiology, 9(4): 451-467.

[36] Murray J.D., 2003. Mathematical Biology. Springer-Verlag.

[37] Neville A.A., Matthews P.C., Byrne, (2006) H.M., Interactions between pattern formation and domain growth. 68: 1975-2003.

[38] Nikolaidou K., Barret K., 2004. A Rho GTPase signaling pathway is used reiteratively in epithelial folding and potentially selects the outcome of Rho activation. Current Biol. 14(20): 1822-1826.

[39] Oster G.F., Murray J.D., Harris K., 1983 Mechanical aspects of mesenchymal morphogenesis. J. Embryol. Exp. Morph. 78: 83-125.

[40] Pouille P.A., Farge E., 2007. Hydrodynamic simulation of multicellular embryo invagination. Phys. Biol., 5/015005.

[41] Pustoc'h A, Ohayon J, Usson Y, Kamgoue A and Tracqui P, 2005. An integrative model of the self-sustained oscillating contractions of cardiac myocytes Acta Biotheoretica, 53:277-293.

[42] Ramasubramamian A. and Taber L.A., 2008. Computational modeling of morphogenesis regulated by mechanical feedback. Biomechan. Model. Mechanobiol. 7, 77-91.

[43] Rauzi M., Lenne P.F. and Lecuit T., 2010. Planar polarized actomyosin contractile flows control epithelial junction remodeling. Nature, 468:1110:1114.

[44] Rodriguez E.K., Hoger A., and McCulloch A.D., 1994. Stress-dependent finite growth in soft elastic tissues. J.Biomechanics, 27:455-46.

[45] Salazar-Ciudad I., Jernvall J., 2010. A computational model of teeth and the developmental origins of morphological variation. Nature, 4654 583-587.

[46] Smith D.R., 1993. An introduction to continuum mechanics. Kluwer Academic Publishers, The Netherlands.

[47] Steward R., 1989. Relocalization of the dorsal protein from the cytoplasm to the nucleus correlates with its function, Cell. Vol. 59, 1179-l 188.

[48] Sun S., Titushkin I., Cho M., 2006. Regulation of mesenchymal stem cell adhesion and orientation in 3D collagen scaffold by electrical stimulus. Bioelectrochemistry, 69:133-141.

[49] Supatto, W., De´barre, D., Moulia, B., Broze´ s, E., Martin, J.L.,Farge, E., 2005. In vivo modulation of morphogenetic movements in Drosophila embryos with femtosecond laser pulses. Proceedings of the National Academic Sciences USA 102 (4),1047–1052.

[50] Sweeton D. et al., 1991. Gastrulation in Drosophila: the formation of the ventral furrow and posterior midgut invaginations. Development, 112: 775-789.

[51] Taber L.A., 1995. Biomechanics of growth, remodeling and morphogenesis. Appl. Mech. Rev., 48(8), 487-545.

[52] Taber L.A., 2007. Theoretical study of Beloussov's hyper-restoration hypothesis for mechanical regulation of morphogenesis. Biomechan. Model. Mechanobiol., 7(6), 727-41.

[53] Turing A.M., 1952. The chemical basis of morphogenesis. Philos. Trans. R. Soc. London B., 327:37-72.

[54] Umilis D., O'Connor M.B., Othmer H.G., 2008. Robustness of embryonic spatial patterning in Drosophila melanogaster. 81: 65-111.

[55] Waddington, C.H., 1940. The genetic control of wing development in Drosophila. J. Genet. 41:75--139.

[56] Weliky M., Oster G., 1990. The mechanical basis of cell rearrangement. Development, 106, 372-386.

[57] Wiebe C., Brodland G.W., 2005. Tensile properties of embryonic epithelia measured using a novel instrument. J. Biomech., 38, 2087-2094.

Figures

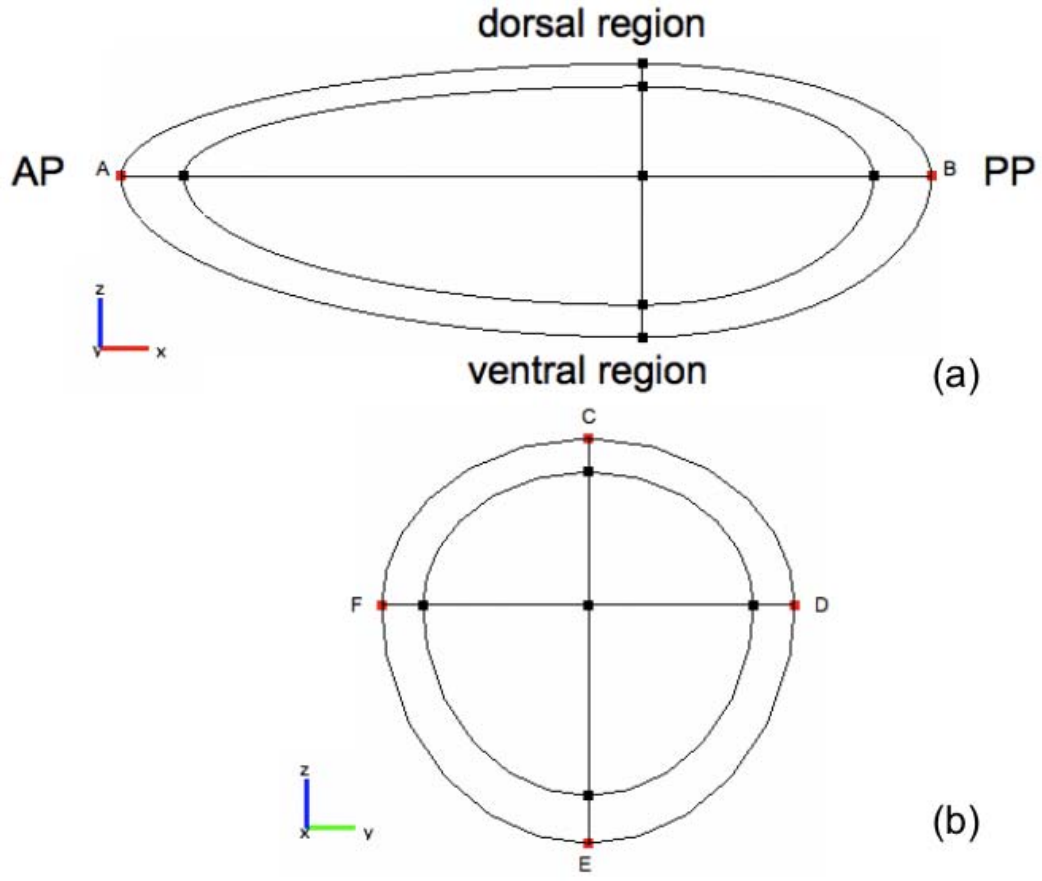

Fig. 1 The geometry of the Drosophila embryo which has been built from an anterior and an exterior ellipsoid retrieved from real embryo images. The major axis AB is *500μm*, while the cross axes CE and DF are respectively *175μm* and *165μm*. The thickness of the embryo varies between $15\mu m < h < 40\mu m$.

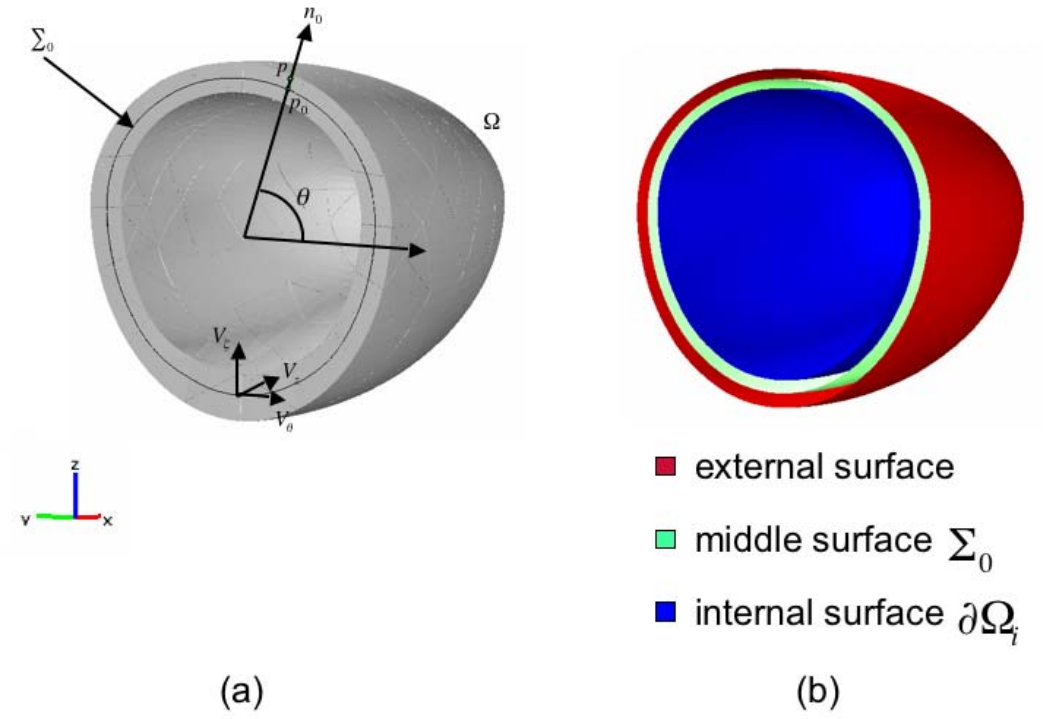

Fig. 2 (a) The curvilinear system of coordinates composed by V_θ, V_z and V_ζ that allows the parameterization of the *Drosophila* geometry. (b) Representation of the external (red), the middle (green) and the internal (blue) surface of the embryo (for sake of clarity, only half of the hollow geometry is reproduced).

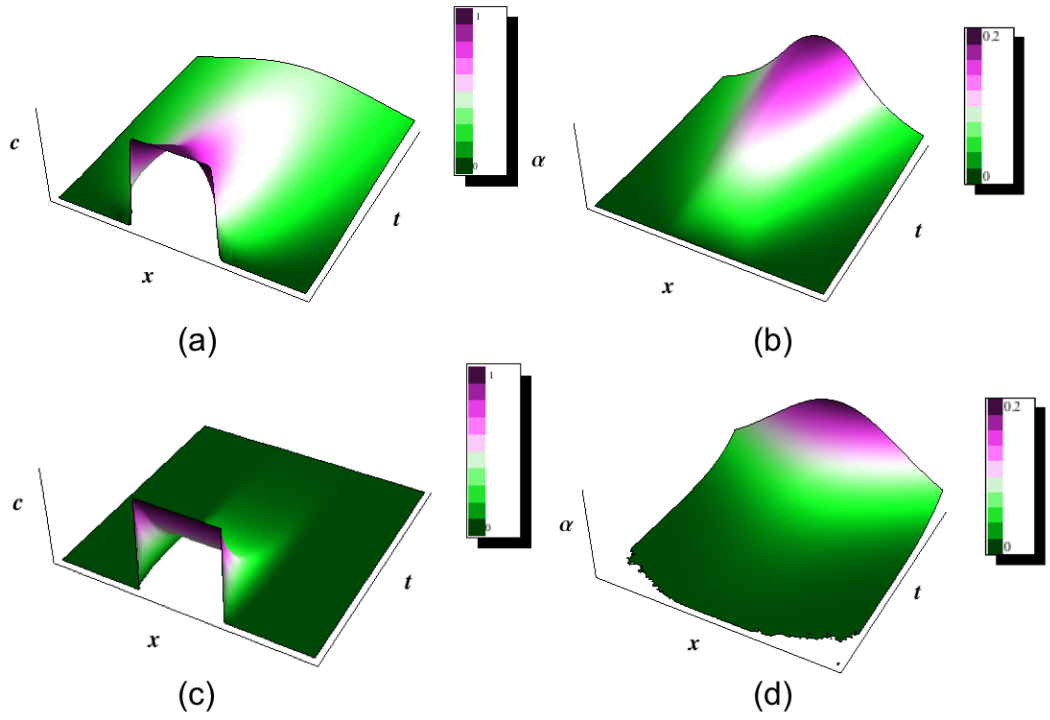

Fig. 3 Evolution of concentration profiles c and intensity factor α as a function of time t and space x for a one-dimensional problem. Initial conditions are: c=1 for $-1<x<1$, and α=0 everywhere. The values of α are governed by the evolution law in Eq (12): $d\alpha/dt=\beta c$ with β=0.1. (a-b) $k_D=1$ and

k_R=0 (c-d) k_D=1 and k_R= -1. In the latter case, there is a morphogen consumption and consequently α grows at slower rate than in case (a-b).

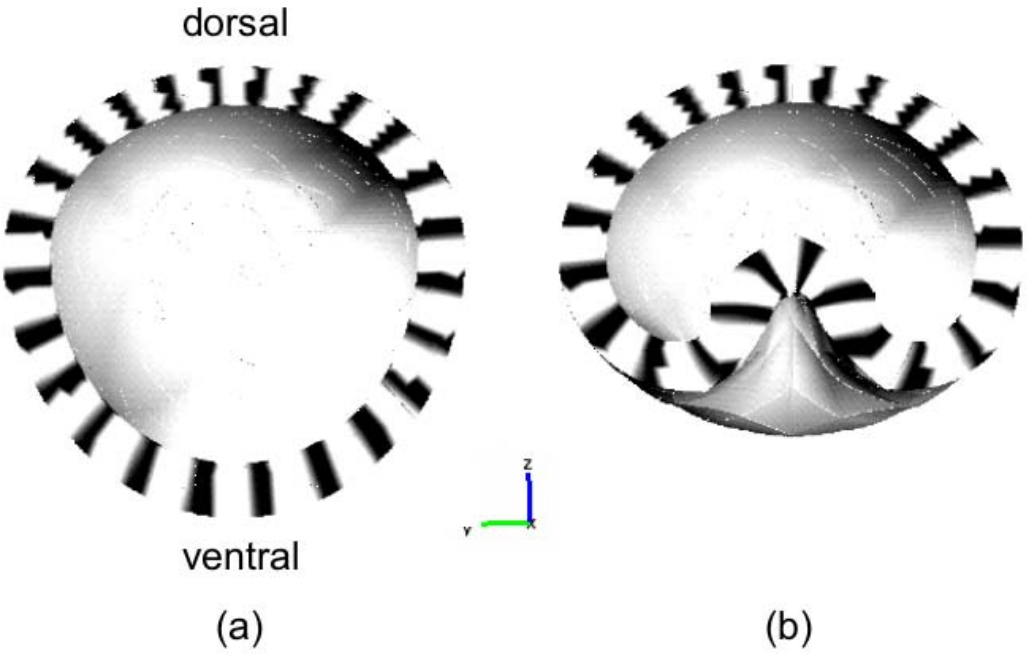

Fig. 4 Representation of the material cells by which the embryonic tissue is subdivided (Eq. (20)) during the VFI simulation. Each white domain represents a cell, while the black domains are triggered by the smoothing effect of the Heaviside function by which the material cells are obtained. (a) Initial configuration (*t=0*): the cells show a columnar shape (b) Final configuration (*t=1s*): the apical constriction has occurred and it is maximal at the apex of the furrow.

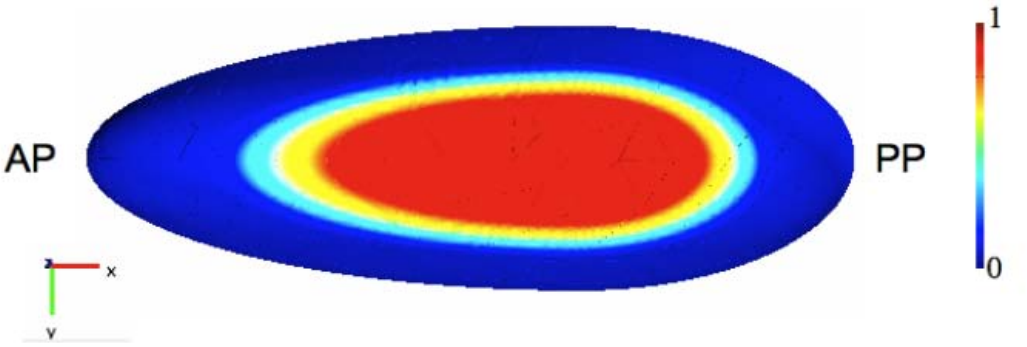

Fig. 5 Isovalues of the concentration *c* at *t=0* for the VFI simulation (ventral view of the embryo).

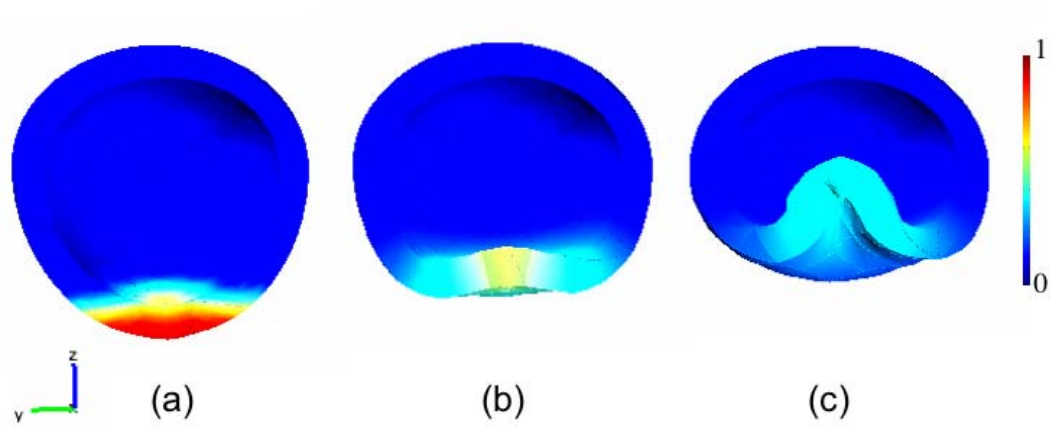

Fig. 6 (a-c) Isovalues of the concentration *c* during the successive steps of the VFI simulation. As we can observe, the morphogen concentration *c* decreases as long as the active deformation increases, so that the VFI occurs.

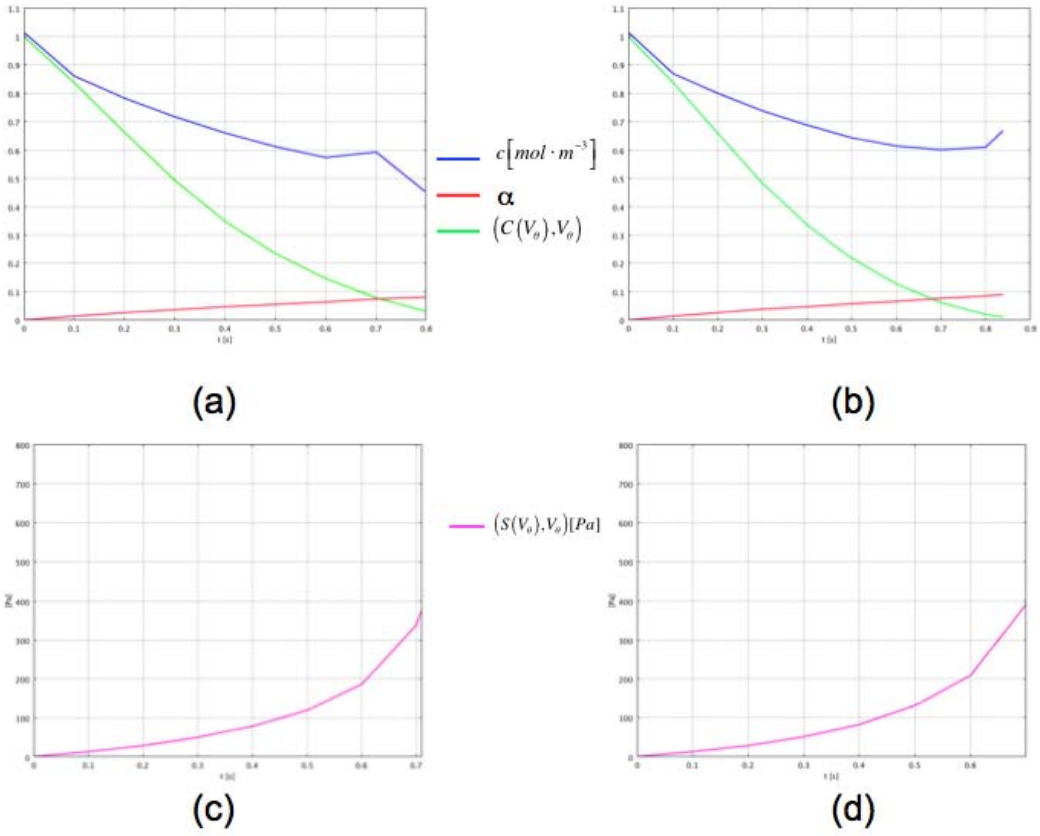

Fig. 7 The trends of the morphogen concentration *c* (blue line), of the active intensity factor α (red line) and of the total apical constriction defined as $\left(C(V_\theta),V_\theta\right)$ (green line) over time *t* during the VFI simulation (the curves are traced for the point E of Fig. 1). In (a) $k_R=0$ and the concentration *c* progressively decreases. In (b), $k_R=0.1s^{-1}$ which leads to an increase of the concentration *c* at the end of the simulation. In both cases, the initial condition at point E is $c=1$ and $\alpha=0$. As expected α always increases. (c) and (d): computation of the stress $\mathbf{S}_m$ along the direction $\boldsymbol{V}_\theta$ (Sec. 4.1) for the case where $k_R=0$ (c) and $k_R=0.1s^{-1}$ (d).

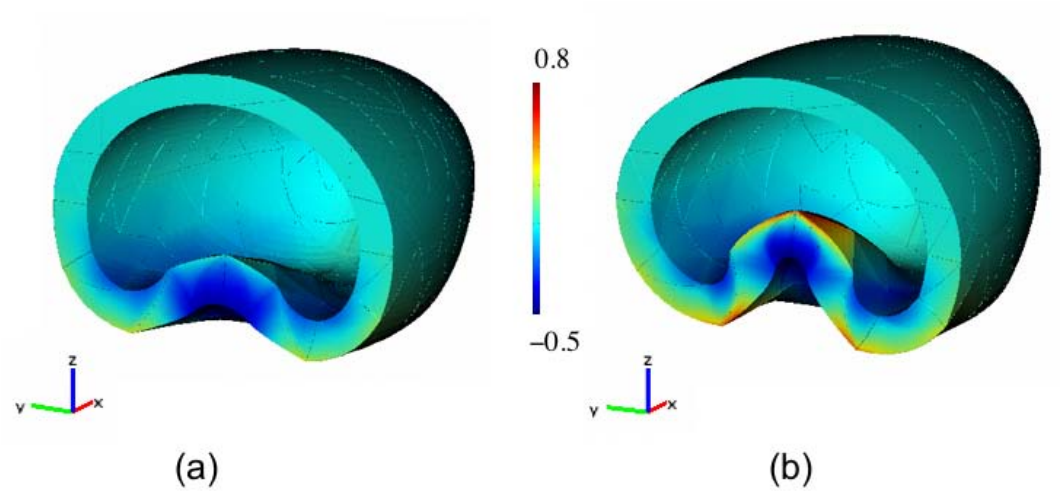

Fig. 8 Final deformation of the tissue during the VFI represented by the projection of the Cauchy-Green tensor $\boldsymbol{C}$ along the tangential vector $\boldsymbol{V}_\theta$ (Eq. (21)). (a) Results when simulating VFI with imposed active deformations, as modeled in [3], yelding a maximal apical constriction equal to 0.32. (b) Present mechano-diffusion simulation of the VFI with a maximal final stretch equal to 0.74.

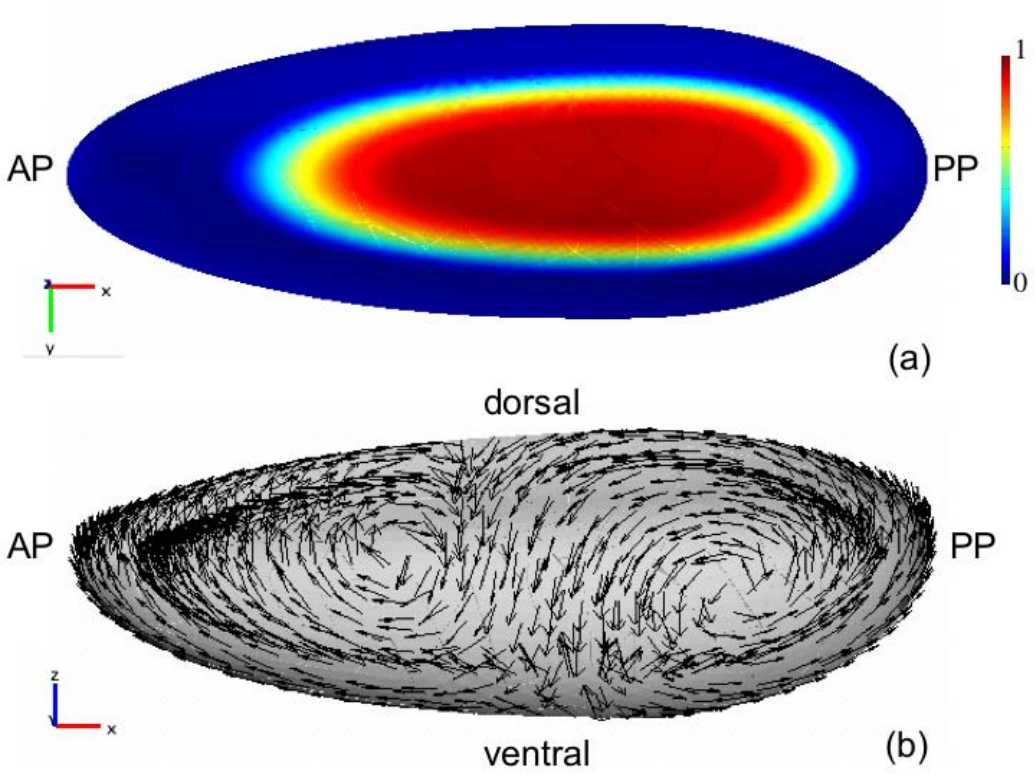

Fig. 9 (a) Isovalues of the concentration c at $t=0$ for the GBE simulation. (ventral view of the embryo). (b) Frontal view of the embryo at the end of the simulation of the GBE ($t=1s$). The black arrows represent the displacement field.

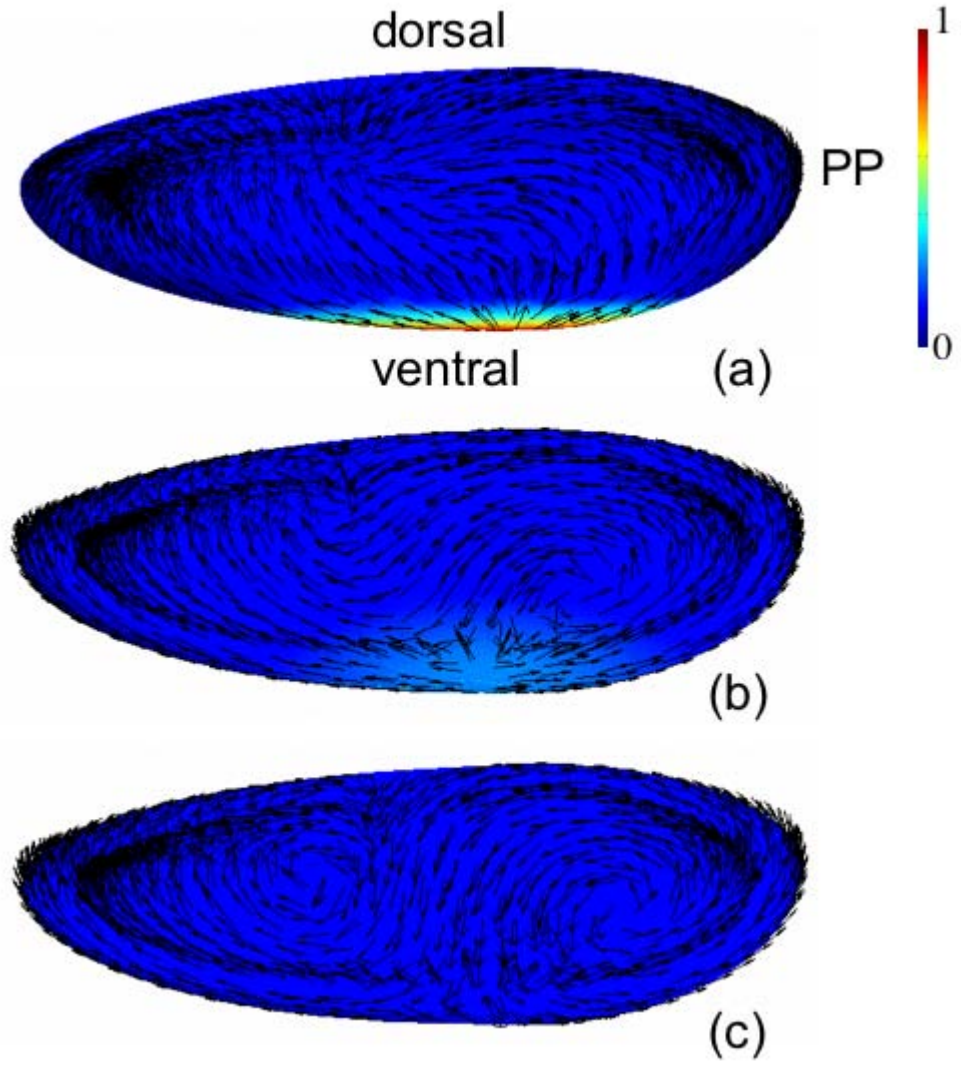

Fig. 10 Frontal views of the embryo. From the top to the bottom, variation of the morphogen concentration *c* during the successive steps of the GBE simulation. The black arrows represent the displacement field.

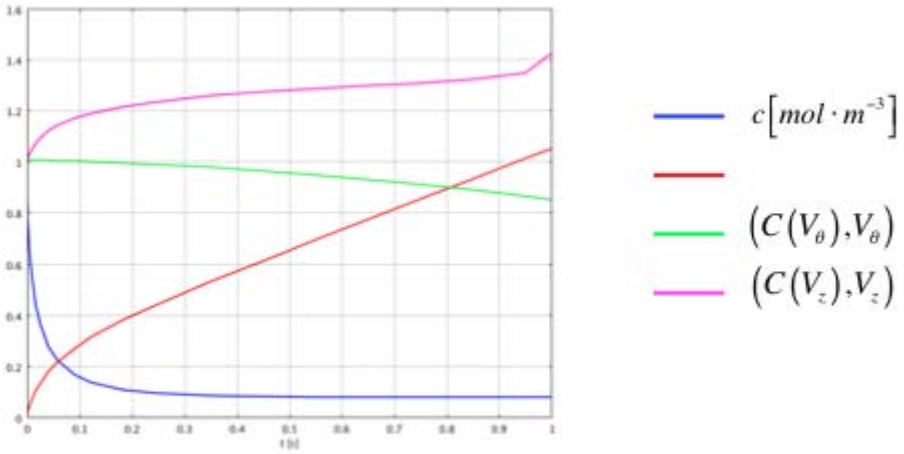

Fig. 11 The trends of the morphogen concentration *c* (blue line), of the active intensity factor α (red line) and of the two active strains: convergence $(C(V_\theta), V_\theta)$ (green line) and extension $(C(V_z), V_z)$ (purple line) over time *t* during the GBE simulation (the curves are traced for the point E of Fig. 1, $k_R=0$). As for the VFI, we observe that the concentration *c* progressively decreases ($c(t=0)=1$), while the active intensity factor α increases ($\alpha(t=0)=0$). The active strains also increase (at $t=0$ they are also equal to 0), but it has to be noticed that the convergence is negative while the extension is positive.